Proteome capacity constraints favor respiratory ATP generation

Authors

Yihui Shen [1,2], Hoang V. Dinh [5], Edward Cruz [2,4], Catherine M. Call [1,2], Heide Baron [2], Rolf-Peter Ryseck [1,2], Jimmy Pratas [1,2], Arjuna Subramanian [2], Zia Fatma [6], Daniel Weilandt [1,2], Sudharsan Dwaraknath [8], Tianxia Xiao [1,2], John I. Hendry [5], Vinh Tran [6], Lifeng Yang [1,2], Yasuo Yoshikuni [8], Huimin Zhao [6,7], Costas D. Maranas [5], Martin Wühr [2,4,*], Joshua D. Rabinowitz [1,2,3,*]

Author affiliations

1 Department of Chemistry, Princeton University, Princeton, NJ, USA

2 Lewis Sigler Institute for Integrative Genomics, Princeton University, Princeton, NJ, USA

3 Ludwig Institute for Cancer Research, Princeton Branch, Princeton, NJ, USA

4 Department of Molecular Biology, Princeton University, Princeton, New Jersey 08544, USA

5 Department of Chemical Engineering, The Pennsylvania State University, University Park, PA, USA

6 Carl R. Woese Institute for Genomic Biology, University of Illinois Urbana-Champaign, Urbana, IL, 61801, USA

7 Department of Chemical and Biomolecular Engineering, University of Illinois at Urbana-Champagne, Urbana, IL, USA

8 US Department of Energy Joint Genome Institute, Lawrence Berkeley National Laboratory, Berkeley, CA 94720, USA

* Corresponding authors

Proteome capacity constraints favor respiratory ATP generation

Abstract

Cells face competing metabolic demands. These include efficient use of both limited substrates and limited proteome capacity, as well as flexibility to deal with different environments. Flexibility requires spare enzyme capacity, which is proteome inefficient. ATP generation can occur via fermentation or respiration. Fermentation is much less substrate-efficient, but often assumed to be more proteome efficient [1–3], thereby favoring fast-growing cells engaging in aerobic glycolysis [4–8]. Here, however, we show that mitochondrial respiration is actually more proteome-efficient than aerobic glycolysis. Instead, aerobic glycolysis arises from cells maintaining the flexibility to grow also anaerobically. These conclusions emerged from an unbiased assessment of metabolic regulatory mechanisms, integrating quantitative metabolomics, proteomics, and fluxomics, of two budding yeasts, *Saccharomyces cerevisiae* and *Issatchenkia orientalis*, the former more fermentative and the latter respiratory. Their energy pathway usage is largely explained by differences in proteome allocation. Each organism's proteome allocation is remarkably stable across environmental conditions, with metabolic fluxes predominantly regulated at the level of metabolite concentrations. This leaves extensive spare biosynthetic capacity during slow growth and spare capacity of their preferred bioenergetic machinery when it is not essential. The greater proteome-efficiency of respiration is also observed in mammals, with aerobic glycolysis occurring in yeast or mammalian cells that maintain a fermentation-capable proteome conducive to both aerobic and anaerobic growth.

Introduction

Metabolism is subject to physical constraints. Given the law of conservation of matter, to maintain homeostasis, limited metabolic inputs must balance with outputs ('flux balance'). These outputs include high energy cofactors (most importantly ATP), building blocks for cell replication, and waste. The resources, including physical space and protein synthesis capacity, to sustain these fluxes are also limited. Thus, cells are under pressure to produce their required metabolic fluxes efficiently. As proteins catalyze most metabolic reactions and comprise the majority of biomass in

55 many cell types, the challenges of limited biosynthetic machinery and physical space can be
56 viewed largely as constraints on proteome capacity [2,3,9–17].
57
58 To manage proteome capacity, cells tailor protein expression to their conditions [18–21]. For example,
59 rapidly growing cells express copious ribosomes [18,22,23]. This requires less expression of other
60 protein types, such as anabolic and catabolic enzymes (e.g. those required for assimilating limiting
61 quantities of nitrogen [24], or breaking down non-preferred carbon sources [21,25]). Conversely, under
62 less favorable conditions, ribosome expression falls to make room for other proteins. Perfect
63 proteome tailoring, however, is not necessarily feasible or desirable [26–30], as proteome remodeling
64 is expensive and spare enzyme capacity can allow cells to quickly ramp up fluxes to deal with
65 changing conditions.
66
67 An important case of metabolic tailoring involves energy production from fermentation versus
68 respiration. Respiration is by far more energy-efficient, producing roughly 10-fold more ATP per
69 glucose [31]. Nevertheless, many organisms ferment, producing organic waste, even when oxygen is
70 available ('aerobic glycolysis'). Aerobic glycolysis is associated with fast growing cells including
71 bacteria, yeast and cancer cells [4–8]. Indeed, as their growth accelerates, both *Escherichia coli* and
72 *S. cerevisiae* switch from respiration to fermentation [2,32].
73
74 Why do cells engage in aerobic glycolysis when it is so much less energy-efficient than respiration?
75 One possibility involves a 'rate-yield tradeoff' [1–3,33]. More specifically, it is often believed that
76 fermentation is capable of producing ATP faster per unit enzyme expression, i.e. more 'proteome
77 efficient' [9–17]. The proteome efficiency of glycolysis versus respiration, however, has not been
78 carefully experimentally tested in eukaryotes.
79
80 Here we examine this question, building from an extensive systems-level analysis of metabolism
81 in two evolutionarily distant budding yeasts (separated by 200 million years [34]): *S. cerevisiae*
82 (Baker's yeast) and *I. orientalis* (also known as *Candida krusei* and *Pichia kudriavzevii*, a species
83 abundant in fermented food, fruit, and soil with favorable properties for bioengineering) [35–40]. We
84 find that, across diverse environmental conditions spanning a broad range of growth rates, the
85 proteome of each yeast varies only modestly, with metabolic flux explained primarily by

86 metabolite levels. Across the yeasts, however, metabolic flux differences are explained mainly by
87 proteome allocation, with *I. orientalis* expressing more respiratory enzymes and outcompeting *S.*
88 *cerevisiae* across diverse aerobic contexts. Both in *I. orientalis* and in respiring *S. cerevisiae*,
89 quantitative measurements show that respiration is actually several-fold more proteome efficient
90 than glycolysis. Similar results are attained in mammalian tissues and cancer cells. The origin of
91 aerobic glycolysis accordingly does not lie in proteome efficiency, but rather in a proteome
92 hedging strategy where cells maintain spare glycolytic capacity in preparation for potential future
93 hypoxia.
94
95 **Results**
96
97 **Metabolic fluxes in *S. cerevisiae* and *I. orientalis***
98 We first characterized aerobic growth and metabolism of *S. cerevisiae* and *I. orientalis* in glucose
99 minimal medium (Fig. S1a). *I. orientalis* grows faster than *S. cerevisiae* (μ = 0.52 vs. 0.39 h^{-1}),
100 respires much more, consumes less glucose, and excretes less ethanol (Fig. S1a). We then resolved
101 flux through the entire metabolic network with ^{13}C metabolic flux analysis (Fig. 1). Specifically,
102 we developed genome-scale metabolic models of both yeasts including complete atom mapping
103 [41]. The models were then constrained by flux balance and experimentally derived extracellular
104 fluxes, biomass fluxes, and isotope labeling (from two distinct ^{13}C-tracer strategies: [1,2-
105 $^{13}C_2$]glucose and [U-$^{13}C_6$]glucose, each at 1:1 molar ratio with unlabeled glucose). This enabled
106 comprehensive yeast metabolic flux analysis, at a rigor previously achieved only in prokaryotes
107 [41,42].
108
109 ^{13}C-tracing resolved key internal flux branch points. For example, [1,2-$^{13}C_2$]glucose revealed
110 markedly higher [M+1] pyruvate labeling in *I. orientalis* (Fig. S1b), reflecting greater oxidative
111 pentose phosphate pathway (PPP) flux in this yeast species (Fig. 1). The same tracer also reveals
112 greater [M+1] tricarboxylic acid (TCA) cycle intermediates in *I. orientalis* (Fig. S1c), consistent
113 with higher oxidative TCA cycle flux relative to *S. cerevisiae*, where clockwise TCA flux was
114 truncated at α-ketoglutarate (Fig. 1). The greatest difference between the two yeasts is in the way
115 glucose is catabolized. Namely, *S. cerevisiae* prefers carbon-inefficient fermentation, and
116 correspondingly makes most ATP from glycolysis and consumes most NADH via ethanol

117 fermentation (Fig. 1, Fig. S1d). In contrast, *I. orientalis* prefers respiration for ATP production,
118 and re-oxidizes NADH by a blend of complex I and the quinone oxidoreductase Nde1, the
119 knockout of which impairs *I. orientalis* but not *S. cerevisiae* growth [43] (Fig. 1, Fig. S1e).
120
121 **Flux control across environmental conditions**
122 When nutrients become scarce, cells adjust metabolic fluxes and growth. Such fluxes can be
123 controlled through enzyme concentration (k_{cat}[E] in the Michaelis-Menten kinetics), active site
124 occupancy ([S]/([S]+K_m)), or allosteric regulation (Fig. 2a). To assess flux control mechanisms in
125 *S. cerevisiae* and *I. orientalis*, we grew each yeast in aerobic chemostats at diverse growth rates
126 controlled by limiting glucose, ammonia, or phosphate availability (Fig. 2b). In each nutrient
127 environment, we measured enzyme concentrations via quantitative proteomics, metabolite
128 concentrations via metabolomics, and metabolic fluxes via ^{13}C-informed fluxomics (Fig. 2c).
129 Fluxes aligned remarkably closely with growth rate in both yeasts (Fig. S2a), with the exception
130 of metabolic switching to respiration and the PPP (relative to glycolysis) in glucose-limited *S.*
131 *cerevisiae*, which renders glucose-limited *S. cerevisiae* metabolically similar to *I. orientalis* (Fig.
132 S2, b and c). On average, 53% of flux variation in *S. cerevisiae* and 71% in *I. orientalis* was
133 explained by growth rate alone.
134
135 The corresponding metabolomics and proteomics data provide a valuable resource for
136 understanding the biochemical basis by which these fluxes are achieved, especially in the non-
137 model yeast. For example, they can be assessed on a reaction-by-reaction basis to identify
138 physiologically meaningful metabolic regulators [44] (Fig. S3a showing glyceraldehyde-3-phosphate
139 dehydrogenase, or GAPD, as an example). We were able to identify allosteric regulation in 19 out
140 of 51 examined reactions in *I. orientalis* (Supplementary Table). Seven of these regulations have
141 also been reported in *S. cerevisiae*, including classical ones such as citrate inhibition of
142 phosphofructokinase [31] and fructose-1,6-bisphosphate activation of pyruvate kinase [45]. Our
143 analysis also revealed multiple previously unappreciated regulatory interactions. For example,
144 ATP inhibits *I. orientalis* GAPD, a novel interaction that we biochemically verified (Fig. S3, a-c).
145 Overall, the integration of *in vivo* enzyme and metabolite concentrations via Michaelis-Menten
146 kinetics explained the vast majority of flux variation across physiological conditions (Fig. 2d).
147 This reflects enzyme concentration, active site occupancy, and allosteric regulation by metabolites

148 collectively accounting for most yeast flux control, without the need to invoke other mechanisms
149 like enzyme covalent modification or localization.
150
151 **Flux control by enzyme concentration**
152 Cells contain extensive programs for regulating protein levels. Across nutrient conditions, however,
153 we observed remarkably stable enzyme concentrations. In contrast, both metabolic fluxes and
154 metabolite concentrations varied much more than enzymes (Fig. 2c, Fig. S2a). For some reactions,
155 enzyme levels even show negative correlation with flux (negative Pearson's R in Fig. 2d with
156 enzyme only). We assessed the extent of physiological flux control residing in enzymes and
157 metabolites based on their metabolic leverage, the product of their physiological concentration
158 variation across conditions and their flux control coefficient based on the best-supported kinetic
159 model from the above quantitative analysis of physiological metabolic regulation. Across 51
160 evaluable reactions, we found that, across nutrient conditions, metabolites exert much more
161 metabolic leverage than enzymes (Fig. 2e, Fig. S3d).
162
163 Indeed, within both yeast species, flux changes across physiological conditions correlate better
164 with pathway substrate concentration changes than pathway enzyme concentration changes (based
165 on median of fold change across pathway components) (Fig. 2, f-i). The maintenance of enzyme
166 concentrations with reduced growth and metabolic flux suggests substantial spare enzyme capacity,
167 which may facilitate rapid growth acceleration when nutrient conditions improve [26,27,46,47].
168
169 In contrast to metabolite-dominant flux control within each yeast in response to changing nutrient
170 environment, flux differences between *S. cerevisiae* and *I. orientalis* strongly aligned with enzyme
171 concentrations (Fig. 2, j-k). Given the 200 million years of evolution separating these two species
172 [34], we expected that there might be substantial differences in enzyme properties that change
173 metabolic flux between the two organisms. Highly expressed proteins, including central metabolic
174 enzymes, however remained strongly conserved between the two yeasts at the protein sequence
175 level (Fig. S4). Correspondingly, enzyme abundances account for a large fraction of flux variation,
176 including the greater glycolysis flux in *S. cerevisiae* and faster TCA turning and oxidative
177 phosphorylation in *I. orientalis* (Fig. 2k). Thus, within the tested yeast species, flux is
178 predominately regulated at the level of metabolite concentrations and active site occupancy. In

179 contrast, flux differences between these yeast species is predominately explained by enzyme
180 concentrations.
181
182 **Proteome-efficiency of ATP generation**
183 We next examined overall proteome allocation of both yeasts with absolute proteomic
184 quantification calibrated by UPS2 standard, and found that metabolic genes (enzymes, transporters,
185 and mitochondrial proteins) together accounted for just over half of the proteome in both species,
186 with the other major proteome sectors being translation (mostly ribosomes) and transcriptional
187 machinery (Fig. 3a). The fractional proteome allocation to these three major sectors was nearly
188 identical across the two yeasts. The major difference was within the metabolic sector, which had
189 three major components: anabolic, glycolytic, and respiratory (the latter being composed of
190 mitochondrial, TCA, and oxidative phosphorylation proteins). The anabolic enzymes constituted
191 a similar proteome fraction in both species, but there was a major reallocation between the two
192 other sectors: *S. cerevisiae* expresses more glycolytic proteins, and *I. orientalis* more respiratory
193 proteins.
194
195 Together, our absolute proteome quantitation and flux analyses enabled quantification of ATP
196 production per protein mass (i.e. proteome efficiency) of glycolysis and respiration in both species.
197 We obtained the ATP flux from the genome-scale model, which included a mechanistic ratio of 3
198 ATP produced for every 10 protons translocated by ATP synthase [48]. Including both TCA and
199 oxidative phosphorylation proteins (but not other mitochondrial proteins) as the proteome cost of
200 respiration, we found that, in batch culture, respiration is more proteome-efficient than glycolysis
201 in both yeasts (Fig. 3b).
202
203 Despite comparing favorably to glycolysis, respiration in glucose-rich batch-cultured *S. cerevisiae*
204 was much less proteome-efficient than in *I.orientalis.* Besides the absence of proton-pumping
205 complex I in *S. cerevisiae*, we hypothesized that this also reflects spare respiratory capacity when
206 glucose is abundant. Consistent with this, the proteome-efficiency of *S. cerevisiae* respiration
207 increased (and of glycolysis fell) under glucose limitation (Fig. 3c, Fig. S5). In contrast, since *I.*
208 *orientalis* defaults to respiration even when glucose is abundant, proteome-efficiency was
209 unaffected by glucose availability.

210

211 Part of glycolytic and TCA flux is diverted to biosynthesis, and glycolytic flux is needed to
212 generate respiratory substrate. We further assessed proteome efficiency of ATP generation of
213 fermentation (turning glucose to ethanol) and respiration (turning glucose to CO_2) by calculating
214 a flux-partitioned proteome cost [2], which counts glycolytic proteins in the cost of respiration and
215 discounts flux diverted to other pathways. In both yeasts, this flux-partitioned analysis identified
216 respiration as the more proteome-efficient ATP production pathway (Fig. S6, a-b). Similarly, even
217 if counting all mitochondrial proteins into respiration's proteome cost, respiration remains more
218 proteome-efficient than glycolysis in *I. orientalis* and glucose-limited *S. cerevisiae* (Fig. S6, c-d).
219

220 **Benefit of aerobic glycolysis**

221 In *S. cerevisiae*, rate-yield tradeoff was believed to underlie the switching to carbon-inefficient
222 fermentation at faster growth [14–17]. Our data reveals, however, that respiration is both more energy-
223 and proteome-efficient than glycolysis. Such efficiency would be expected to lead to greater fitness.
224

225 Consistently, *I. orientalis* outcompetes *S. cerevisiae* in co-culture under conditions requiring
226 respiratory ATP production (ethanol, glucose limitation). Importantly, however, it also
227 outcompetes under conditions where fermentation is a viable strategy (abundant glucose, nitrogen
228 limitation, phosphorus limitation, and even sucrose as the sole carbon source, which *S. cerevisiae*
229 can ferment on while *I. orientalis* alone cannot metabolize and presumably takes in glucose and
230 fructose liberated by *S. cerevisiae*) (Fig. 4a, Fig. S7).
231

232 If respiration is both more energy- and proteome-efficient than glycolysis, why does aerobic
233 glycolysis occur? One possibility is the production of a toxic product that impairs competitors:
234 ethanol [49,50]. Another is carbon resource competition, essentially quick uptake of glucose [1,33,51].
235 These might help *S. cerevisiae* compete with bacteria, but did not against *I. orientalis* (Fig. 4a).
236

237 We wondered whether the benefit of aerobic glycolysis might instead not be during aerobic growth,
238 but rather in hedging for oxygen limitation (hypoxia) [13]. *S. cerevisiae* was repeatedly exposed to
239 oxygen limitation during human baking and winemaking [52]. But oxygen limitation can also occur
240 readily naturally, due to oxygen's limited solubility ($c_{O2} \approx 230\ \mu$mol/L) and slow diffusion in water

241 ($D \approx 2.3\times10^{-9}$ m^2/s). We measured the dissolved oxygen at the bottom of unstirred *S. cerevisiae*
242 and *I. orientalis* cultures, and found that oxygen depletion occurred at relatively low culture
243 density (Fig. S8). Notably, *S. cerevisiae* outcompeted *I. orientalis* in fully or cyclically oxygen-
244 depleted co-cultures (Fig. 4a, Fig. S7). Consistently, we observed about 60% growth rate reduction
245 in *I. orientalis* but not *S. cerevisiae* upon oxygen depletion or pharmacological inhibition of
246 electron transport chain complex III by antimycin (Fig. 4b). Both oxygen depletion and antimycin
247 increased glucose uptake rate by more than two-fold in *I. orientalis* (Fig. 4c), which is mediated
248 by about 3-fold higher expression of glycolytic proteins (Fig. 4d). Notably, this glycolytic protein
249 expression came at the expense of ribosomal proteins, consistent with the growth defect in
250 anaerobic *I. orientalis* (Fig. 4d, Fig. S9).
251
252 **Proteomic hedging and aerobic glycolysis**
253 Both *I. orientalis* and *S. cerevisiae* can tailor their respiratory versus glycolytic enzyme expression
254 to environmental conditions. But this tailoring is incomplete: *I. orientalis* partially retains
255 respiratory enzyme and mitochondrial protein expression in hypoxia (Fig. 4d), while *S. cerevisiae*
256 retains high glycolytic enzymes in aerobic conditions (Fig. 2g).
257
258 To explore the consequences of incomplete proteome tailoring, we assembled a coarse-grained
259 quantitative model of yeast growth and metabolism, where growth is limited both by ATP
260 generation (fermentative or respiratory) and by translational machinery, jointly constrained by
261 proteome capacity (Fig. 4e and Extended Data Note). Growth optimization is performed to find
262 the optimal respiratory and glycolytic proteome allocation (f_R and f_G, respectively). This minimal
263 model captures the proteome tradeoff between optimal aerobic and anaerobic growth (Fig. 4e).
264 While optimal aerobic growth is achieved via respiratory ATP production, when the proteome is
265 constrained to always contain enough glycolytic enzyme for rapid anaerobic growth, aerobic
266 glycolysis emerges as an optimal strategy (Fig. 4f).
267
268 **Mammalian ATP generation**
269 We were curious if the greater proteome efficiency of respiration generalizes from yeast to
270 mammals. To investigate this, we quantified the proteome efficiency of glycolysis and respiration
271 in cultured cancer cells and mouse tissues (Fig. 5). ATP flux was from previous reports or

272 estimated based on reported oxygen consumption rates [54,55] (Fig. 5a). The proteome fraction
273 allocated to glycolysis and respiration was computed from published proteomics data [56,57], which
274 shows that mouse tissues in general have greater respiratory proteome capacity like in *I. orientalis*,
275 whereas cancer cell lines have more glycolytic proteome like in *S. cerevisiae* (Fig. 5b). Overall,
276 the proteome efficiency of both glycolysis and respiration was lower in mammals than in yeast,
277 consistent with mammals being under less stringent selection for proteome efficiency.
278 Nevertheless, in both cultured cancer cells and *in vivo* tissues, respiration was the more proteome-
279 efficient ATP generation pathway (Fig. 5c). Thus, in both yeast and mammals, mitochondrial
280 respiration is more proteome-efficient than glycolysis.
281
282 **Discussion**
283 Here we report in-depth proteomic, metabolomic, and metabolic flux characterization of two
284 divergent budding yeasts across various environmental conditions. The resulting data reveal
285 principles of yeast metabolism and its regulation. Prior integrative 'omic analysis of *E. coli* and *S.*
286 *cerevisiae* concluded that metabolism is substantially 'self-regulated', i.e. that changes in
287 metabolic flux are caused more by metabolites themselves than transcriptional and translational
288 reprogramming of enzyme levels [44,58–60]. This conclusion is reinforced by analogous analysis of *I.*
289 *orientalis* here, which shows even less proteome variation across most environmental conditions
290 than *S. cerevisiae,* and yet greater dominance of metabolic flux control by metabolites themselves.
291
292 In contrast to the limited impact of the proteome on flux control within each species, across the
293 two species, metabolic differences are mainly encoded by protein abundances. Given that these
294 two yeasts diverged roughly 200 million years ago, the ability to explain most of their metabolic
295 differences through enzyme concentrations – rather than changes in the properties of enzymes
296 themselves – is notable, and speaks to the importance of proteome allocation in driving metabolic
297 divergence even across long timescales [61].
298
299 The most striking metabolic difference between *I. orientalis* and *S. cerevisiae* is that, in the
300 presence of abundant glucose, the former respires while the latter engages in aerobic glycolysis.
301 We show that, across a wide range of aerobic conditions, the more respiratory yeast grows faster
302 and has superior competitive fitness. This aligns with respiration requiring less of the cell's

303 precious proteome capacity to achieve the same growth-required ATP flux. Quantitative analysis
304 of mammalian cancer cells and tissues demonstrates that respiration is also more proteome-
305 efficient than glycolysis in mammals.
306
307 Prior careful evaluation of proteome efficiency in *E. coli* reached a seemingly opposite conclusion,
308 finding that acetate fermentation is favored for its proteome efficiency [2]. Acetate overflow
309 metabolism in *E. coli*, however, involves a blend of glycolytic and respiratory ATP generation
310 with 4 NADH feeding into the electron transport chain for each glucose. This provides an ATP
311 yield of about 12 per glucose, the majority of which is made via the oxidative phosphorylation
312 (compared to 2 ATP per glucose in yeast or mammalian aerobic glycolysis). Thus, aerobic
313 'fermentation' in *E. coli* is proteome efficient only because it generates substantial respiratory ATP.
314
315 Overall, supported by our data in *S. cerevisiae* and *I. orientalis*, we propose that cells of a given
316 type tend to have a characteristic metabolic proteome that varies only modestly across conditions.
317 In this nearly fixed enzyme network, changing substrate levels induce different fluxes, providing
318 metabolic flexibility without the need for extensive proteome remodeling. A benefit of such
319 proteome constancy is that cells are prepared in advance for changing metabolic environments.
320 One of the most important metabolic fluctuations cells face is shifting oxygen availability [62]. We
321 thus posit that aerobic glycolysis occurs not because it is beneficial per se, but as a side effect of
322 maintaining a fermentative proteome that effectively supports both aerobic and anaerobic growth.
323

324 **Reference**

325 1. Pfeiffer, T., Schuster, S. & Bonhoeffer, S. Cooperation and Competition in the Evolution of
326 ATP-Producing Pathways. *Science* **292**, 504–507 (2001).
327 2. Basan, M. *et al.* Overflow metabolism in Escherichia coli results from efficient proteome
328 allocation. *Nature* **528**, 99–104 (2015).
329 3. Molenaar, D., van Berlo, R., de Ridder, D. & Teusink, B. Shifts in growth strategies reflect
330 tradeoffs in cellular economics. *Mol. Syst. Biol.* **5**, 323 (2009).
331 4. Crabtree, H. G. Observations on the carbohydrate metabolism of tumours. *Biochem. J.* **23**,
332 536–545 (1929).
333 5. De Deken, R. H. The Crabtree Effect: A Regulatory System in Yeast. *J. Gen. Microbiol.* **44**,
334 149–156 (1966).
335 6. Vander Heiden, M. G., Cantley, L. C. & Thompson, C. B. Understanding the Warburg Effect:
336 The Metabolic Requirements of Cell Proliferation. *Science* **324**, 1029–1033 (2009).
337 7. DeBerardinis, R. J. & Chandel, N. S. We need to talk about the Warburg effect. *Nat. Metab.*
338 **2**, 127–129 (2020).
339 8. Wolfe, A. J. The Acetate Switch. *Microbiol. Mol. Biol. Rev.* **69**, 12–50 (2005).
340 9. Adadi, R., Volkmer, B., Milo, R., Heinemann, M. & Shlomi, T. Prediction of Microbial
341 Growth Rate versus Biomass Yield by a Metabolic Network with Kinetic Parameters. *PLoS*
342 *Comput. Biol.* **8**, e1002575 (2012).
343 10. O'Brien, E. J., Lerman, J. A., Chang, R. L., Hyduke, D. R. & Palsson, B. Ø. Genome- scale
344 models of metabolism and gene expression extend and refine growth phenotype prediction.
345 *Mol. Syst. Biol.* **9**, 693 (2013).
346 11. Mori, M., Hwa, T., Martin, O. C., De Martino, A. & Marinari, E. Constrained Allocation Flux
347 Balance Analysis. *PLOS Comput. Biol.* **12**, e1004913 (2016).

348 12. Salvy, P. & Hatzimanikatis, V. The ETFL formulation allows multi-omics integration in
349 thermodynamics-compliant metabolism and expression models. *Nat. Commun.* **11**, 30 (2020).
350 13. Wortel, M. T., Noor, E., Ferris, M., Bruggeman, F. J. & Liebermeister, W. Metabolic enzyme
351 cost explains variable trade-offs between microbial growth rate and yield. *PLOS Comput. Biol.*
352 **14**, e1006010 (2018).
353 14. Sánchez, B. J. *et al.* Improving the phenotype predictions of a yeast genome-scale metabolic
354 model by incorporating enzymatic constraints. *Mol. Syst. Biol.* **13**, 935 (2017).
355 15. Oftadeh, O. *et al.* A genome-scale metabolic model of Saccharomyces cerevisiae that
356 integrates expression constraints and reaction thermodynamics. *Nat. Commun.* **12**, 4790
357 (2021).
358 16. Elsemman, I. E. *et al.* Whole-cell modeling in yeast predicts compartment-specific proteome
359 constraints that drive metabolic strategies. *Nat. Commun.* **13**, 801 (2022).
360 17. Chen, Y. & Nielsen, J. Energy metabolism controls phenotypes by protein efficiency and
361 allocation. *Proc. Natl. Acad. Sci.* **116**, 17592–17597 (2019).
362 18. You, C. *et al.* Coordination of bacterial proteome with metabolism by cyclic AMP signalling.
363 *Nature* **500**, 301–306 (2013).
364 19. Li, G.-W., Burkhardt, D., Gross, C. & Weissman, J. S. Quantifying Absolute Protein Synthesis
365 Rates Reveals Principles Underlying Allocation of Cellular Resources. *Cell* **157**, 624–635
366 (2014).
367 20. Dekel, E. & Alon, U. Optimality and evolutionary tuning of the expression level of a protein.
368 *Nature* **436**, 588–592 (2005).
369 21. Keren, L. *et al.* Massively Parallel Interrogation of the Effects of Gene Expression Levels on
370 Fitness. *Cell* **166**, 1282-1294.e18 (2016).

371 22. Bosdriesz, E., Molenaar, D., Teusink, B. & Bruggeman, F. J. How fast-growing bacteria
372 robustly tune their ribosome concentration to approximate growth-rate maximization. *FEBS J.*
373 **282**, 2029–2044 (2015).
374 23. Peebo, K. *et al.* Proteome reallocation in Escherichia coli with increasing specific growth rate.
375 *Mol. Biosyst.* **11**, 1184–1193 (2015).
376 24. Hui, S. *et al.* Quantitative proteomic analysis reveals a simple strategy of global resource
377 allocation in bacteria. *Mol. Syst. Biol.* **11**, 784 (2015).
378 25. Gancedo, J. M. Yeast Carbon Catabolite Repression. *Microbiol. Mol. Biol. Rev.* **62**, 334–361
379 (1998).
380 26. Metzl-Raz, E. *et al.* Principles of cellular resource allocation revealed by condition-dependent
381 proteome profiling. *eLife* **6**, e28034 (2017).
382 27. O'Brien, E. J., Utrilla, J. & Palsson, B. O. Quantification and Classification of E. coli Proteome
383 Utilization and Unused Protein Costs across Environments. *PLOS Comput. Biol.* **12**, e1004998
384 (2016).
385 28. Yu, R. *et al.* Nitrogen limitation reveals large reserves in metabolic and translational capacities
386 of yeast. *Nat. Commun.* **11**, 1881 (2020).
387 29. Postma, E., Verduyn, C., Scheffers, W. A. & Van Dijken, J. P. Enzymic analysis of the crabtree
388 effect in glucose-limited chemostat cultures of Saccharomyces cerevisiae. *Appl. Environ.*
389 *Microbiol.* **55**, 468–477 (1989).
390 30. Christodoulou, D. *et al.* Reserve Flux Capacity in the Pentose Phosphate Pathway Enables
391 Escherichia coli's Rapid Response to Oxidative Stress. *Cell Syst.* **6**, 569-578.e7 (2018).
392 31. Lehninger, A. L., Nelson, D. L. & Cox, M. M. *Lehninger principles of biochemistry*. (W.H.
393 Freeman, 2005).

394 32. Van Hoek, P., Van Dijken, J. P. & Pronk, J. T. Effect of Specific Growth Rate on Fermentative
395 Capacity of Baker's Yeast. *Appl. Environ. Microbiol.* **64**, 4226–4233 (1998).
396 33. Bachmann, H. *et al.* Availability of public goods shapes the evolution of competing metabolic
397 strategies. *Proc. Natl. Acad. Sci.* **110**, 14302–14307 (2013).
398 34. Shen, X.-X. *et al.* Tempo and Mode of Genome Evolution in the Budding Yeast Subphylum.
399 *Cell* **175**, 1533-1545.e20 (2018).
400 35. Radecka, D. *et al.* Looking beyond *Saccharomyces* : the potential of non-conventional yeast
401 species for desirable traits in bioethanol fermentation. *FEMS Yeast Res.* **15**, fov053 (2015).
402 36. Fatma, Z., Schultz, J. C. & Zhao, H. Recent advances in domesticating non-model
403 microorganisms. *Biotechnol. Prog.* **36**, (2020).
404 37. Xiao, H., Shao, Z., Jiang, Y., Dole, S. & Zhao, H. Exploiting Issatchenkia orientalis SD108
405 for succinic acid production. *Microb. Cell Factories* **13**, 121 (2014).
406 38. Suthers, P. F. *et al.* Genome-scale metabolic reconstruction of the non-model yeast
407 Issatchenkia orientalis SD108 and its application to organic acids production. *Metab. Eng.*
408 *Commun.* **11**, e00148 (2020).
409 39. Cao, M. *et al.* A genetic toolbox for metabolic engineering of Issatchenkia orientalis. *Metab.*
410 *Eng.* **59**, 87–97 (2020).
411 40. Douglass, A. P. *et al.* Population genomics shows no distinction between pathogenic Candida
412 krusei and environmental Pichia kudriavzevii: One species, four names. *PLOS Pathog.* **14**,
413 e1007138 (2018).
414 41. Gopalakrishnan, S. & Maranas, C. D. 13C metabolic flux analysis at a genome-scale. *Metab.*
415 *Eng.* **32**, 12–22 (2015).

416 42. McCloskey, D., Young, J. D., Xu, S., Palsson, B. O. & Feist, A. M. Modeling Method for
417 Increased Precision and Scope of Directly Measurable Fluxes at a Genome-Scale. *Anal. Chem.*
418 **88**, 3844–3852 (2016).
419 43. Luttik, M. A. H. *et al.* The Saccharomyces cerevisiae NDE1 and NDE2 Genes Encode
420 Separate Mitochondrial NADH Dehydrogenases Catalyzing the Oxidation of Cytosolic
421 NADH. *J. Biol. Chem.* **273**, 24529–24534 (1998).
422 44. Hackett, S. R. *et al.* Systems-level analysis of mechanisms regulating yeast metabolic flux.
423 *Science* **354**, aaf2786–aaf2786 (2016).
424 45. Schomburg, D., Schomburg, I. & Chang, A. *Springer handbook of enzymes*. (Springer, 2007).
425 46. Reznik, E. *et al.* Genome-Scale Architecture of Small Molecule Regulatory Networks and the
426 Fundamental Trade-Off between Regulation and Enzymatic Activity. *Cell Rep.* **20**, 2666–2677
427 (2017).
428 47. Jansen, M. L. A. *et al.* Prolonged selection in aerobic, glucose-limited chemostat cultures of
429 Saccharomyces cerevisiae causes a partial loss of glycolytic capacity. *Microbiology* **151**,
430 1657–1669 (2005).
431 48. Symersky, J. *et al.* Structure of the c10 ring of the yeast mitochondrial ATP synthase in the
432 open conformation. *Nat. Struct. Mol. Biol.* **19**, 485–491 (2012).
433 49. Zhou, N. *et al.* Coevolution with bacteria drives the evolution of aerobic fermentation in
434 Lachancea kluyveri. *PLOS ONE* **12**, e0173318 (2017).
435 50. Dashko, S., Zhou, N., Compagno, C. & Piškur, J. Why, when, and how did yeast evolve
436 alcoholic fermentation? *FEMS Yeast Res.* **14**, 826–832 (2014).
437 51. MacLean, R. C. & Gudelj, I. Resource competition and social conflict in experimental
438 populations of yeast. *Nature* **441**, 498–501 (2006).

439 52. Dekker, W. J. C., Wiersma, S. J., Bouwknegt, J., Mooiman, C. & Pronk, J. T. Anaerobic
440 growth of *Saccharomyces cerevisiae* CEN.PK113-7D does not depend on synthesis or
441 supplementation of unsaturated fatty acids. *FEMS Yeast Res.* **19**, foz060 (2019).
442 53. Martin, A. W. & Fuhrman, F. A. The Relationship between Summated Tissue Respiration and
443 Metabolic Rate in the Mouse and Dog. *Physiol. Zool.* **28**, 18–34 (1955).
444 54. Zielinski, D. C. *et al.* Systems biology analysis of drivers underlying hallmarks of cancer cell
445 metabolism. *Sci. Rep.* **7**, 41241 (2017).
446 55. Bartman, C. R. *et al. Slow TCA flux implies low ATP production in tumors*.
447 http://biorxiv.org/lookup/doi/10.1101/2021.10.04.463108 (2021)
448 doi:10.1101/2021.10.04.463108.
449 56. Wang, M., Herrmann, C. J., Simonovic, M., Szklarczyk, D. & Mering, C. Version 4.0 of
450 PaxDb: Protein abundance data, integrated across model organisms, tissues, and cell-lines.
451 *PROTEOMICS* **15**, 3163–3168 (2015).
452 57. Gholami, A. M. *et al.* Global Proteome Analysis of the NCI-60 Cell Line Panel. *Cell Rep.* **4**,
453 609–620 (2013).
454 58. Fendt, S. *et al.* Unraveling condition-dependent networks of transcription factors that control
455 metabolic pathway activity in yeast. *Mol. Syst. Biol.* **6**, 432 (2010).
456 59. Millard, P., Smallbone, K. & Mendes, P. Metabolic regulation is sufficient for global and
457 robust coordination of glucose uptake, catabolism, energy production and growth in
458 Escherichia coli. *PLOS Comput. Biol.* **13**, e1005396 (2017).
459 60. Gerosa, L. *et al.* Pseudo-transition Analysis Identifies the Key Regulators of Dynamic
460 Metabolic Adaptations from Steady-State Data. *Cell Syst.* **1**, 270–282 (2015).

461 61. Kito, K. *et al.* Yeast Interspecies Comparative Proteomics Reveals Divergence in Expression
462 Profiles and Provides Insights into Proteome Resource Allocation and Evolutionary Roles of
463 Gene Duplication. *Mol. Cell. Proteomics* **15**, 218–235 (2016).
464 62. Dewhirst, M. W., Cao, Y. & Moeller, B. Cycling hypoxia and free radicals regulate
465 angiogenesis and radiotherapy response. *Nat. Rev. Cancer* **8**, 425–437 (2008).
466
467 **Acknowledgement**
468
469 We thank the members of Rabinowitz lab for discussion on experiments and the manuscript; S.
470 Silverman and J. Avalos for yeast strains, L. Ryazanova for help with proteomics experiment, P.
471 F. Suthers for discussion on the genome-scale model, M. Gupta for discussion on protein
472 regulation, N. Piyush and Z. Zhang for advice on competitive fitness, and Z.-Y. Wu for
473 experimental support. This work was funded by DOE grant DE-SC0018260 and the DOE Center
474 for Advanced Bioenergy and Bioproducts Innovation (Award Number DE-SC0018420). Any
475 opinions, findings, conclusions or recommendations expressed in this publication are those of the
476 author(s) and do not necessarily reflect the views of the U.S. Department of Energy.
477
478 **Author contributions**
479
480 Y.S., M.W. and J.D.R. designed this study. Y.S. performed most of the experiments and data
481 analysis. H.V.D. designed and performed genome-scale metabolic flux analysis with the input
482 from Y.S., J.I.H., and C.D.M. E.C., H.B., and A.S. performed proteomics measurement. C.M.C.
483 performed nutrient limited culture and measurement. R.P.R. designed and performed enzyme
484 purification and qPCR. J.P. performed enzyme purification and competitive growth experiments.
485 Z.F. created mutant yeast strains with the input from H.Z., and contributed to enzyme purification.
486 S.D. and Y.Y. contributed to yeast growth measurement. V.T. contributed to enzyme purification.
487 T.X. contributed to metabolomics measurements. D.W. contributed to enzyme constrained
488 modeling. L.Y. contributed to oxygen consumption measurement. Y.S. and J.D.R. wrote the
489 manuscript with input from all co-authors.

490

491
492

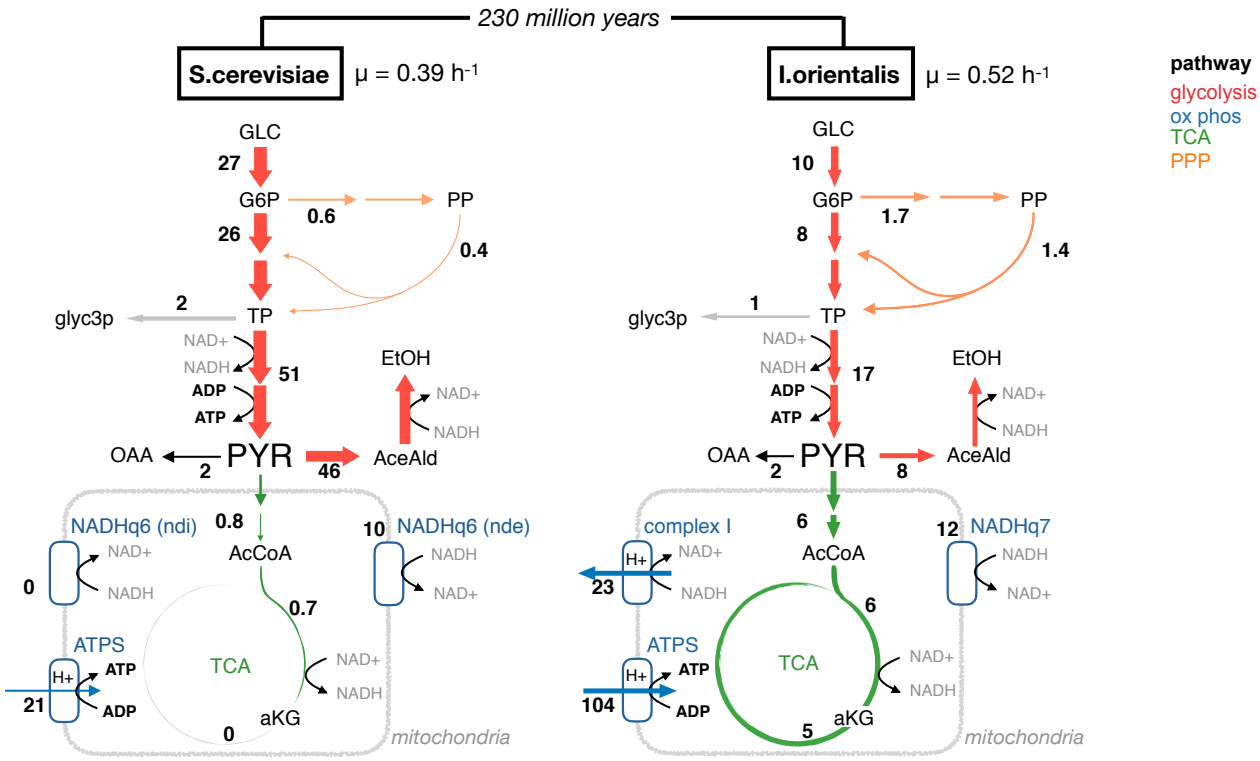

Figure 1. Genome-scale flux analysis shows more active respiratory metabolism in *I. orientalis*.

Metabolic flux (in mmol/gDW/h) of *S. cerevisiae* (CEN.PK) and *I. orientalis* (SD108) in aerobic exponential growth in YNB with 20 g/L glucose. Fluxes are best estimate from genome-scale ^{13}C-informed metabolic flux analysis (MFA), with the input data including metabolite ^{13}C labeling from two ^{13}C-glucose tracers (each with n = 3 or 4 biological replicates) and consumption and excretion fluxes (at least n = 3 biological replicates). Color represents metabolic pathways: glycolysis in red, oxidative phosphorylation (ox phos) in blue, TCA in green, and PPP in orange. Numbers represents flux in mmol/h/gDW.

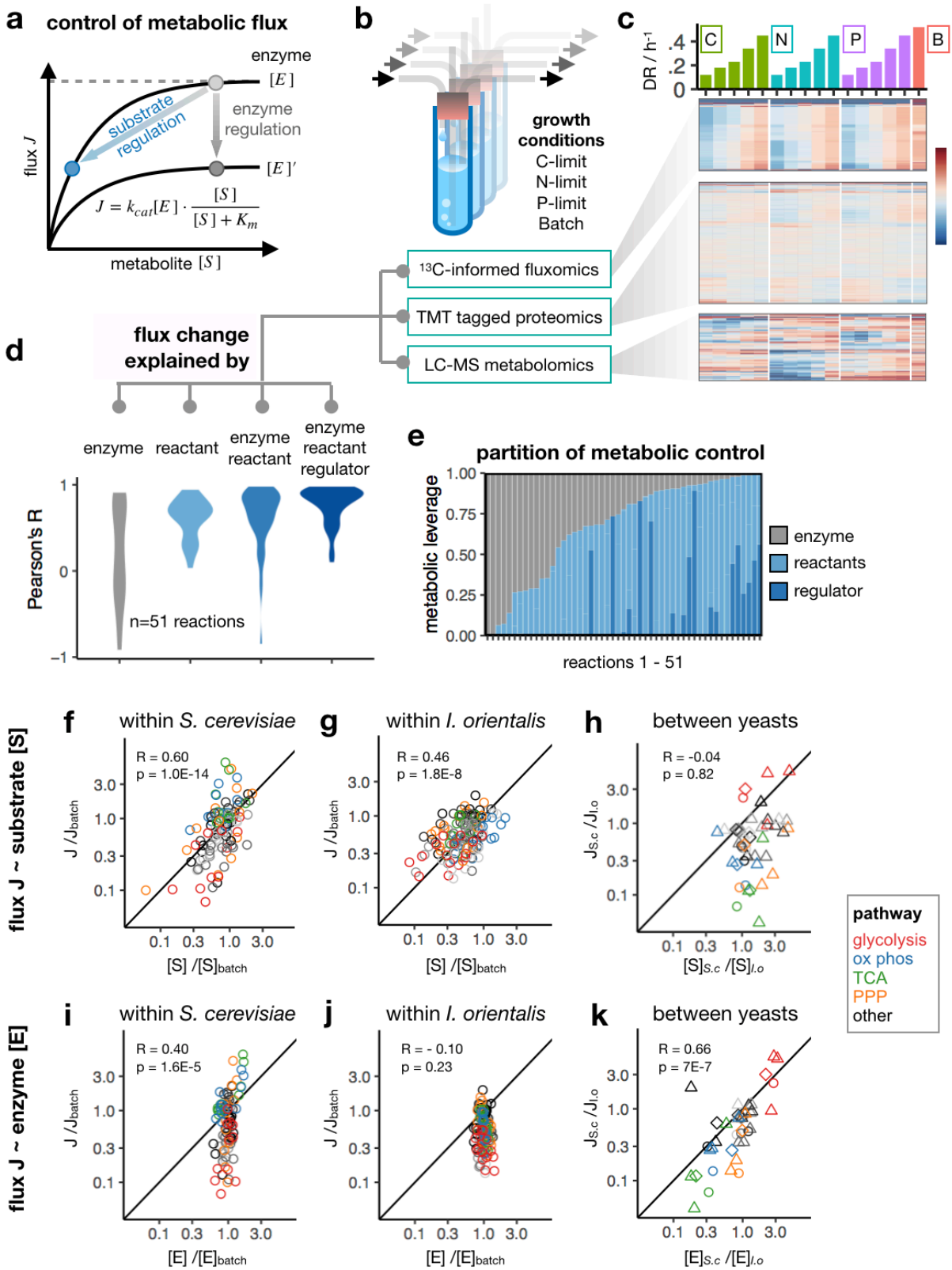

Figure 2. Flux change is explained by metabolites within yeast species, and by enzymes across yeasts. (Legend continues on next page.)

508 **Figure 2. Flux change is explained by metabolites within yeast species, and by enzymes across**
509 **yeasts.**
510 (a) Flux change can be achieved through change in either enzyme or substrate level via Michaelis-
511 Menten kinetics.
512 (b) Multi-omics data were obtained in steady-state yeast grown in nutrient-limited continuous
513 culture or nutrient-replete batch culture.
514 (c) Genome-wide metabolic flux, protein abundance, and metabolite concentrations in *I. orientalis*
515 across growth conditions. Values are normalized to the geometric mean across all the conditions.
516 Metabolomics, mean of n = 3 technical replicates (independent sampling from continuous culture).
517 Proteomics, n = 1 biological replicate. Fluxomics, best estimates from ^{13}C-MFA similar to Fig. 1.
518 (d) Distribution of Pearson's R for 51 reactions between measured flux and flux predicted from
519 Michaelis-Menten kinetics accounting for different variables: concentration of enzyme, reactant,
520 and best data-supported allosteric regulator (if any).
521 (e) Partition of metabolic control among enzyme, reactants, and regulator for 51 reactions in *I.*
522 *orientalis*.
523 (f-k) Correlation between flux and metabolite concentration (f-h) or between flux and enzyme
524 concentration (i-k). Data within an organism (f,g,i,j) compares nutrient limited to batch conditions.
525 Data across organisms (h,k) compares *S. cerevisiae* to *I. orientalis.* Each point represents median
526 flux and concentration fold change for the pathway. Pearson's R and p value are shown. Symbols
527 in (h, k) are diamonds, CEN.PK in batch culture; circle, FY4 in batch culture; triangle, FY4 in
528 nutrient limitation at 0.22 h^{-1}. Black line shows slope = 1. Other pathways (folate, sugar, nucleic
529 acid, lipid, amino acid) are plotted in different shades of grey.
530
531

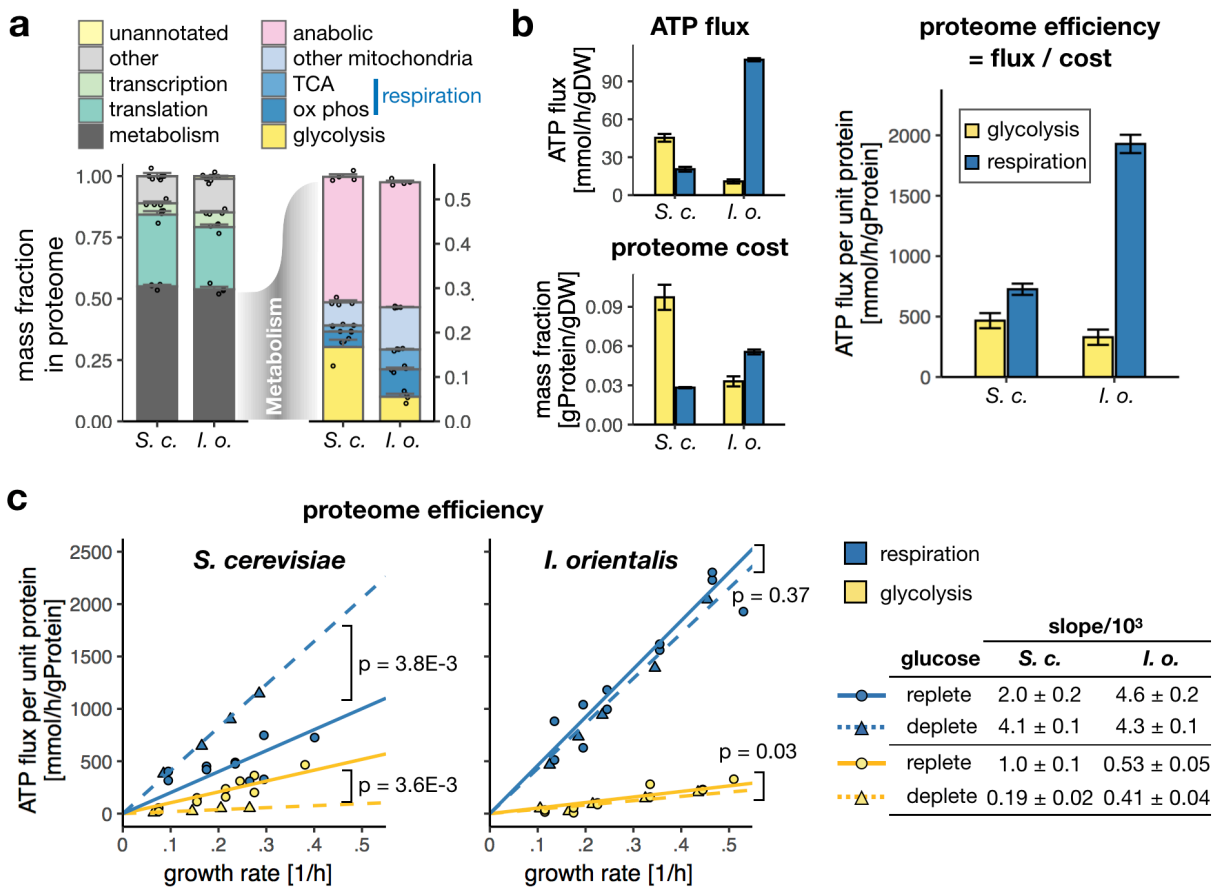

Figure 3. Proteome efficiency across nutrient conditions in *S.cerevisiae* and *I. orientalis*.

(a) Proteome allocation of *S. cerevisiae* (CEN.PK) and *I. orientalis* in exponentially growing batch culture. Mean ± SE, n = 4 biological replicates.

(b) ATP fluxes (from ^{13}C-informed MFA), proteome mass fraction (of whole cell dry weight), and proteome efficiency for glycolysis and respiration in exponentially growing aerobic glucose-fed batch culture. ATP fluxes are shown as mean ± SE based on ^{13}C-MFA confidence interval. Proteome efficiency is shown as mean ± SE, with error propagated from flux and proteome fraction measurements.

(c) Proteome efficiency of respiration and glycolysis across different nutrient conditions in *S. cerevisiae* (left) and *I. orientalis* (right). For raw data, see Fig. S5. Solid line shows linear regression in glucose replete conditions (Batch, N-limit, and P-limit). Dashed line is glucose-depleted conditions (C-limit). P values are from ANOVA of linear model.

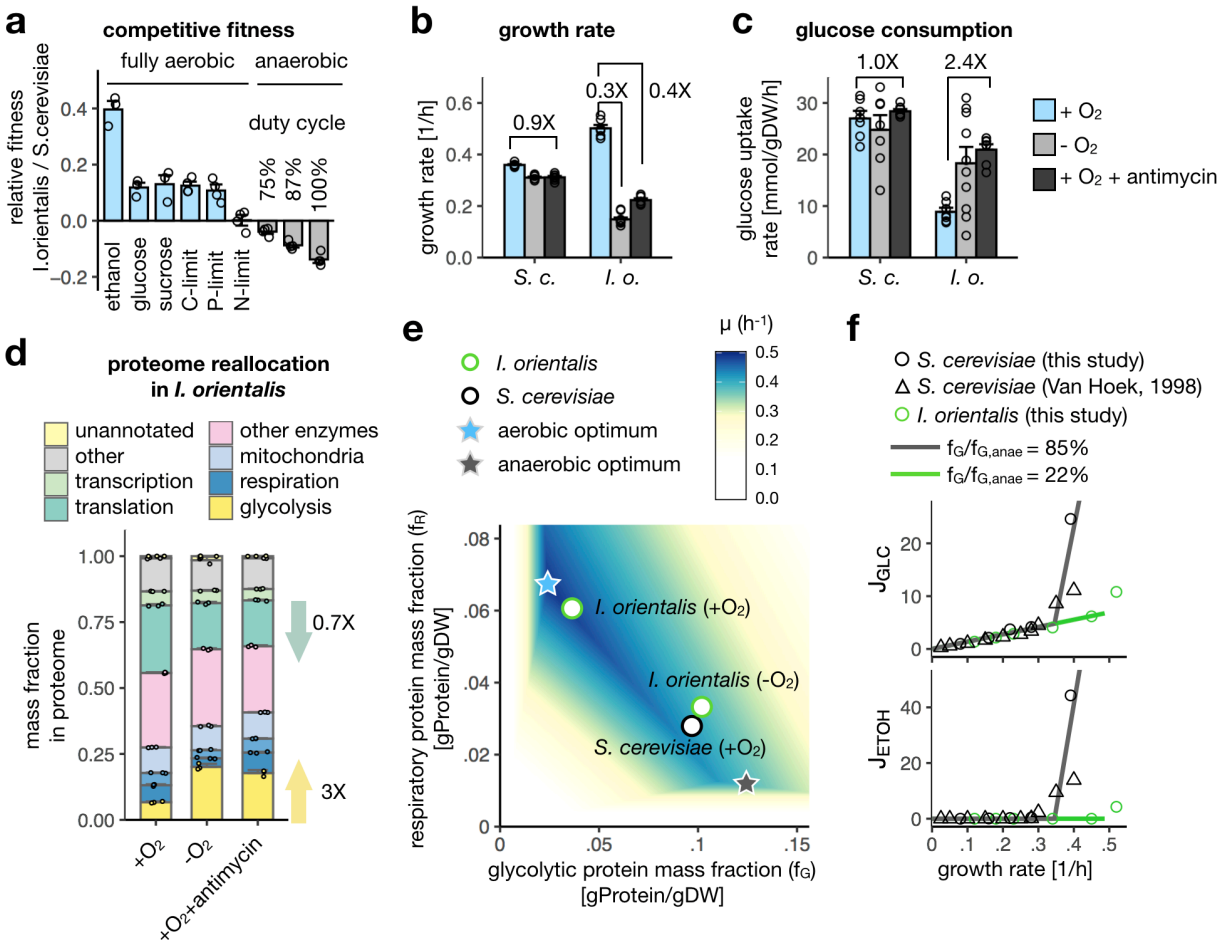

546

547 **Figure 4. Aerobic glycolysis emerges from anaerobically primed proteome.**

548 (a) Fitness of *I. orientalis* and *S. cerevisiae* measured in competitive co-culture. Relative
549 abundance of the two yeasts was measured by qPCR at 4 to 6 time points and used to obtain fitness.
550 See method for details. Mean ± SE, n = 3 or 4 biological replicates.

551 (b-c) Specific growth rates (b) and glucose consumption rates (c) for batch-cultured *S. cerevisiae*
552 and *I. orientalis* with oxygen (blue), without oxygen (light grey), and with 10 μM antimycin (dark
553 grey). Mean ± SE, n = 6 or 7 biological replicates.

554 (d) Proteome allocation in *I. orientalis* in above conditions. Mean ± SE, n=3 biological replicates.
555 Arrows show fold change in translational and glycolytic proteome compared to aerobic condition.

556 (e) Respiro-fermentative growth rate (μ) was predicted from a proteome-constrained coarse-
557 grained model parameterized with proteome efficiency measured from *S. cerevisiae*. Glycolytic
558 (f_G) and respiratory proteome fraction (f_R), are mass fractions of whole cell dry weight. Optimal
559 proteome fractions in aerobic and anaerobic condition were indicated as stars. Measured proteome

560 fractions in glucose-fed batch cultures of *I. orientalis* (aerobic, $+O_2$; or anaerobic, $-O_2$) and *S.*
561 *cerevisiae* (aerobic, $+O_2$) are shown in circles.
562 (f) Experimental glucose consumption (J_{GLC}) and ethanol excretion (J_{ETOH}) rates (symbols, in
563 mmol/h/gDW) and prediction from proteome-constrained model (lines) under high (*S. cerevisiae*)
564 or low (*I. orientalis*) glycolytic capacity (f_G relative to its anaerobic optimum, $f_{G,anae}$). Literature
565 data was obtained from Van Hoek 1998 [32].
566

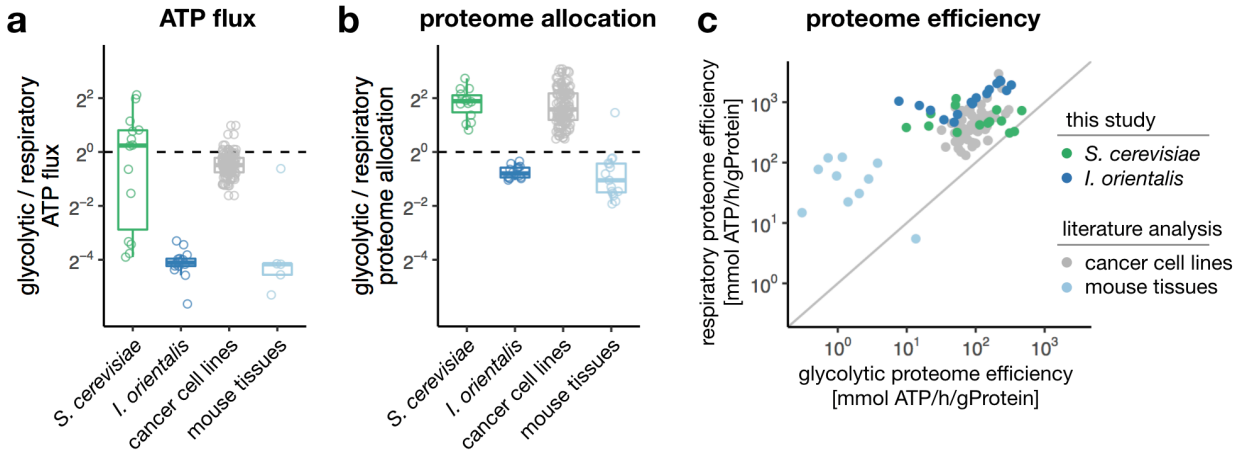

Figure 5. Respiratory ATP production is more proteome efficient than glycolysis in mammals.

(a) Ratio between glycolytic and respiratory ATP production in *I. orientalis*, *S. cerevisiae*, NCI60 cancer cell lines, and mouse tissues. For yeasts, each data point represents a nutrient condition. For cancer cell lines and mouse tissues, each point represents an individual cell line or tissue.

(b) As in (a), for proteome allocation.

(c) Corresponding glycolytic versus respiratory proteome efficiency.